Zonal-mean global teleconnection from 15 to 110 km derived from SABER and WACCM

Bo Tan,[1] Xinzhao Chu,[1] Han-Li Liu,[2] Chihoko Yamashita,[1,2] and James M. Russell III[3]

Received 21 August 2011; revised 11 April 2012; accepted 11 April 2012; published 17 May 2012.

[1] We derive the correlation patterns over the global latitudes and from the stratosphere to lower thermosphere (broadly referred to as teleconnection) using temperature data measured by the Sounding of the Atmosphere using Broadband Emission Radiometry (SABER) from 2002 to 2010, and using 54 years of simulations of temperatures and winds by the Whole Atmosphere Community Climate Model (WACCM). We also analyze the possible mechanisms of teleconnection by investigating the correlations between the temperature and residual circulation. The correlation patterns show that teleconnection exists globally over the equatorial, mid- and high-latitudes, and temperature anomalies correspond well to the anomalies of the residual circulations through adiabatic heating/cooling. A main new finding of this study is that the teleconnection extends well into the lower thermosphere, the thermospheric anomalies are consistent with the corresponding changes of the winter-to-summer lower-thermospheric branch of the residual circulation, and the winter stratosphere perturbations influence the thermosphere globally. Using a reference point chosen in the northern winter stratosphere, we find that the teleconnection structures for time periods with and without Sudden Stratospheric Warmings (SSWs) display similar patterns in SABER, and teleconnection patterns in WACCM are nearly identical for days with major SSWs, minor SSWs and without SSWs. WACCM results show strong inter-annual and intra-annual altitude variations of the teleconnection patterns in the southern polar region but stable altitudes of correlation regions in the equatorial and northern latitudes. The altitude variations are likely responsible for the weak correlations poleward of 60°S when multiyear or multimonth data are used.

Citation: Tan, B., X. Chu, H.-L. Liu, C. Yamashita, and J. M. Russell III (2012), Zonal-mean global teleconnection from 15 to 110 km derived from SABER and WACCM, *J. Geophys. Res.*, *117*, D10106, doi:10.1029/2011JD016750.

1. Introduction

[2] Coupling of the atmosphere over altitudes and latitudes is important to understand the impacts of the lower atmosphere on the middle and upper atmosphere. For example, inter-hemispheric coupling between the northern winter polar stratosphere and southern summer polar mesosphere was first noted by *Becker and Schmitz* [2003]. In their paper, a general circulation model was used to study how the winter mesosphere responds to a planetary wave anomaly in the winter troposphere and lower stratosphere. Heating in the summer mesosphere and lower thermosphere (MLT) at all latitudes south of 60°N and cooling in the winter mesosphere north of 30°N are produced along with warming of the winter stratosphere during periods when planetary wave activity is increased. Adiabatic heating and direct heating caused by breaking of internal gravity waves are believed to contribute to the temperature change in the mesosphere. It is found from this modeling study that below 0.01 hPa adiabatic heating dominates, while at higher altitudes and between 30°N and 60°N, the direct gravity wave heating overcompensates for the changes in dynamic heating [*Becker and Schmitz*, 2003]. However, the mechanism of inter-hemispheric coupling was not clearly identified in this paper. *Becker et al.* [2004] and *Becker and Fritts* [2006] used a general circulation model to reproduce the temperature and wind anomalies observed by rocket measurements in the northern summer mesosphere at Andoya in 2002. They provide model and experimental evidence showing that those anomalies are linked to enhanced planetary Rossby-wave activity in the austral winter troposphere during June–August through inter-hemispheric coupling. *Karlsson et al.* [2009a] used a comprehensive middle atmosphere model, the Canadian Middle Atmosphere Model (CMAM), to reproduce inter-hemispheric coupling and to identify possible mechanisms. They argue that the mechanism behind inter-hemispheric coupling is a series of

[1]Cooperative Institute for Research in Environmental Sciences and Department of Aerospace Engineering Sciences, University of Colorado Boulder, Boulder, Colorado, USA.
[2]High Altitude Observatory, National Center for Atmospheric Research, Boulder, Colorado, USA.
[3]Center for Atmospheric Sciences, Hampton University, Hampton, Virginia, USA.

Corresponding author: B. Tan, Cooperative Institute for Research in Environmental Sciences, University of Colorado Boulder, Boulder, CO 80302, USA. (bo.tan@colorado.edu)

0148-0227/12/2011JD016750

wave-mean flow interactions, triggered by the planetary wave activity in the winter troposphere and stratosphere. The anomaly of planetary-wave forcing in the winter stratosphere produces an anomaly of zonal wind and induces a gravity wave drag (GWD) anomaly in the winter mesosphere through the change of filtering conditions. This GWD anomaly will in turn lead to an anomaly of the mesospheric pole-to-pole circulation. The anomaly of this circulation causes a heating or cooling anomaly in the equatorial mesosphere and this heating or cooling anomaly produces a thermal unbalance in the summer hemisphere. To reach balance again, the zonal wind in the summer polar region will be modified such that the filtering of mesospheric gravity waves is changed, which will affect the temperature in the summer mesosphere. *Körnich and Becker* [2010] confirmed the mechanism of inter-hemispheric coupling using a zonally symmetric model that excluded any additional effects due to resolved waves and non-zonally propagating gravity waves. They have pointed out that gravity waves in the summer hemisphere at latitudes higher than 30 deg are essential for inter-hemispheric coupling while gravity waves around the equator are not.

[3] *Karlsson et al.* [2007, 2009b], *Xu et al.* [2009], *Gumbel and Karlsson* [2011] and *Espy et al.* [2011] provide observational evidence of inter-hemispheric coupling. *Karlsson et al.* [2007] found anti-correlations between the effective optical radius of polar mesospheric clouds (PMCs) in the summer hemisphere and temperature given by the European Centre for Medium-Range Weather Forecasts (ECMWF) in the winter stratosphere. The PMC effective radius and ECMWF temperature they used were monthly averages in July or January from 2002 to 2007. *Karlsson et al.* [2009b] used daily PMC frequencies from the Aeronomy of Ice in the Mesosphere (AIM) satellite during the Southern Hemisphere (SH) 2007–2008 summer, daily zonal-mean temperature profiles from the Microwave Limb Sounder (MLS), and zonal mean winds from the Goddard Earth Observing System (GEOS-5) in the Northern Hemisphere (NH) to study inter-hemispheric coupling. They found positive/negative correlations between SH PMC frequency and NH stratospheric zonal wind/temperature. The results indicate that intraseasonal PMC variability is, in large measure, caused by inter-hemispheric coupling [*Karlsson et al.*, 2009b]. *Xu et al.* [2009] formed the correlation patterns of 4 independent years using MLS temperature data, where the correlations are taken between the southern summer mesosphere temperature at 0.002 hPa from 80° to 85°S and the temperatures elsewhere. This is similar to the methods used by *Karlsson et al.* [2009a], although the extent of the MLS data sets was still insufficient to fully reveal inter-annual variations of teleconnection patterns. Utilizing 9 years of Odin satellite observations of PMC occurrence frequency to represent the state of the summer mesosphere and ECMWF temperature and wind to represent stratosphere conditions, *Gumbel and Karlsson* [2011] showed the seasonal behavior of the summer mesosphere being affected by both intra and inter-hemispheric coupling processes. *Espy et al.* [2011] confirmed the inter-hemispheric coupling between the polar summer mesosphere and planetary-wave activity in the extratropical winter stratosphere using a 10-year time series of summer mesospheric temperatures near 60°N derived from OH nightglow. Their time-lagged correlation between the OH temperatures and the ECMWF winter stratospheric temperatures displayed a strong Quasi-Biennial Oscillation (QBO).

[4] In the current work, we further study the correlation patterns over latitudes and from the stratosphere to the lower thermosphere (herein referred to as teleconnection) using SABER temperature data and WACCM simulations of temperatures and winds. We also analyze the possible mechanisms of teleconnection by investigating the correlations between the residual circulation and temperature. A new finding of this study is that the teleconnection extends well into the lower thermosphere, and the thermospheric anomalies are consistent with the corresponding changes of the winter-to-summer lower-thermospheric branch of the residual circulation. We examine the teleconnection for periods with and without SSWs using a reference point chosen in the northern winter stratosphere (instead of southern summer mesosphere in previous studies) in order to be consistent with the definition of a SSW. Furthermore, the 54 years of WACCM simulation results are used to calculate annual and monthly correlation patterns and analyze the inter-annual and intra-annual variations of each response region. The data and simulations are briefly described in section 2, followed by the analysis and results in section 3.

2. Data and Simulations

[5] The SABER instrument, aboard the Thermosphere, Ionosphere, Mesosphere, Energetics, and Dynamics (TIMED) satellite, measures infrared radiance coming from the Earth's limb in the 4.3 μm and 15 μm CO_2 bands to retrieve temperatures over the 15–110 km altitude range with 2 km vertical resolution. The orbital plane of the TIMED satellite precesses slowly because of its 74 deg orbital inclination. It takes 60 days for SABER to cover all local times [*Russell et al.*, 1999; *Remsberg et al.*, 2004]. The data are sampled at different longitudes due to the rotation of the Earth relative to the orbital plane and at different latitudes due to the motion of the satellite along the orbit. SABER began its observations in January 2002. We use temperature data from 2002 to 2010 (version 1.07), and calculate zonal mean temperature for each day. For our purpose of examining the teleconnection with and without SSW, four northern winter months (November through February) are desired for this study. However, because of the TIMED 60-day yaw cycle, SABER only covers the high northern latitudes in winter from mid January to mid March. Consequently, the data used in this study include the ~60-day period from mid January to mid March for each year.

[6] The NCAR WACCM model extends from the ground to 140 km [*Garcia et al.*, 2007]. In this study, we use daily mean temperature and wind profiles at each longitude and latitude calculated using a free running simulation of WACCM 3.5 for the period of 1953 to 2006. In WACCM 3.5, there are 66 pressure levels from 1000 hPa to 1×10^{-5} hPa and the model altitude intervals change with altitude. The intervals are ~1 and 3 km at 20 and 100 km, respectively. WACCM 3.5 employs a new scheme of gravity wave parameterization as described in *Richter et al.* [2008, 2010]. According to *Richter et al.* [2010], WACCM3.5 does not produce a QBO internally. QBO is imposed by nudging the tropical wind to observations based on *Balachandran*

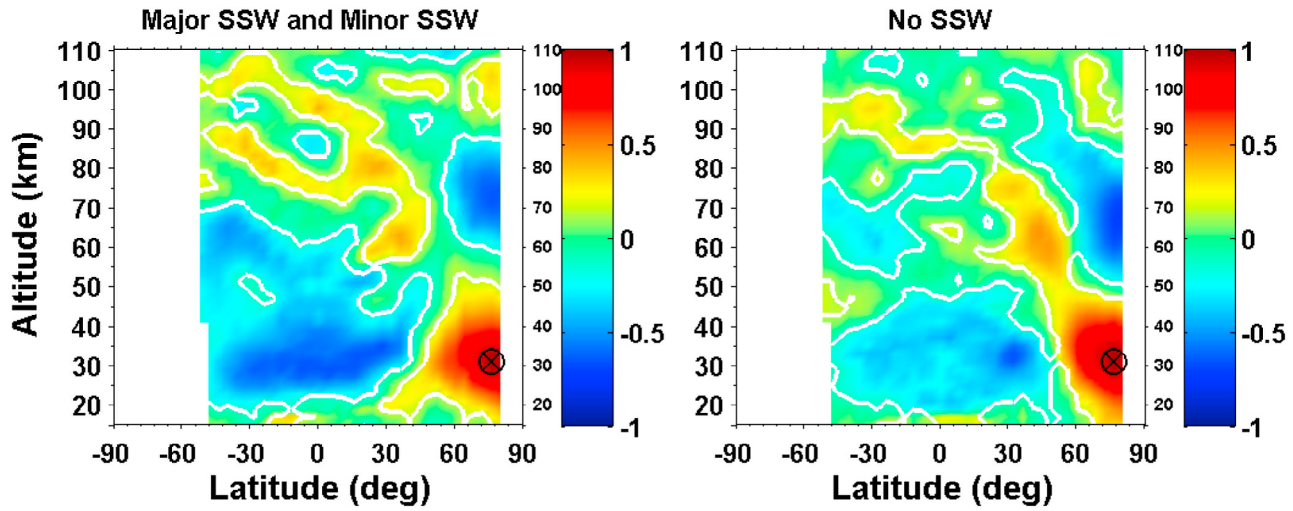

Figure 1. Correlation patterns between the deseasonalized SABER temperature series at a reference point (10 hPa, 76°N) and at all other latitudes and altitudes for days (left) with SSWs and (right) without SSWs. The circle with a cross is the reference point used for the correlation calculations. White solid lines denote the 95% significance level.

and Rind [1995]. At each latitude, zonal mean temperature is calculated at each pressure surface. Residual circulation is calculated using the following equation (equations (3.5.1) of *Andrews et al.*, [1987]):

$$V = \bar{v} - \rho_o^{-1}\left(\frac{\rho_o \overline{v'\theta'}}{\bar{\theta}_z}\right)_z \quad \text{and} \quad W = \bar{w} + (a\cos\phi)^{-1}\left(\cos\phi\frac{\overline{v'\theta'}}{\bar{\theta}_z}\right)_\phi$$

where V and W are the meridional and vertical components of the residual circulation; $\bar{v}$ and $\bar{w}$ are the zonal mean meridional and vertical wind velocities; $\overline{v'\theta'}$ is eddy heat flux, ϕ is latitude, a is the mean radius of the Earth, and ρ_o is atmosphere density at the height of interest. Note that the z in above equation is a log-pressure height, and a scale height of 7 km is used to convert the WACCM output pressure to the log-pressure height z. As mentioned above, to examine the correlations for different SSW periods, the four northern winter months (November through February) are desired for this study. Further considering the analysis for time lags of −10 to +10 days, extra 10 days in October and in March respectively are included to ensure that the lag analysis has all four months of winter covered. Therefore, the simulation data used in this study are from October 20 to March 10 for each year. Note that tidal aliasing may be present in the derived zonal-mean temperature of SABER, but such aliasing has been removed in WACCM zonal means. Since the correlation patterns of SABER and WACCM are similar in general as shown in Section 3, it is most likely that tides are not a dominant factor in the correlation.

3. Analysis and Results

3.1. Teleconnection Analysis

[7] Zonal means derived from SABER data (from mid January to mid March) are used to study teleconnection. At each latitude and altitude (with resolutions of 4 deg and 2 km), the long-term average of daily zonal-mean temperature for each day-of-year (DOY) is obtained by taking the average of the 9 years of SABER data on the same DOY. The temperature anomalies at each latitude and altitude for all 9 years are then calculated as the deviations from the long-term average of daily mean temperatures at that latitude and altitude. These anomalies are used to calculate the correlations between a chosen reference point (10 hPa, 76°N) and all other latitudes and altitudes. All the SABER data during northern winters are separated into two categories: category 1 contains all the episodes with SSW events (both major and minor SSWs), and category 2 contains all the days without SSWs. Here a SSW event is identified using the National Center for Environmental Prediction (NCEP) temperatures at (10 hPa, 80°N). An event with the NCEP temperature increasing more than 25 K within three weeks is defined as a SSW, and all days within this temperature peak are taken as the days of this SSW. For each latitude and altitude, the temperature series in category 1 contains the SABER temperature anomalies on all days during SSWs, and all 9 years of temperature data in category 1 are combined into one array. All 9 years of temperature anomalies in category 2 are combined into one array using the same methods. The major and minor SSWs were included in the same category because there are not enough data to calculate the correlations for major and minor SSWs separately. Figure 1 shows the correlation patterns calculated from SABER data for days with and without SSWs, respectively. The white contour lines in Figure 1 indicate the 95% level of significance. In general, the regions with larger correlation magnitudes have significant levels above 95%, while the smaller correlation regions (close to zero) with colors close to green are insignificant. Both cases show very similar correlation patterns for the regions with significant levels above 95%, but the correlation magnitudes are different. The absolute values of correlation coefficients for days with SSWs are larger than for those without SSWs. This is expected because temperature

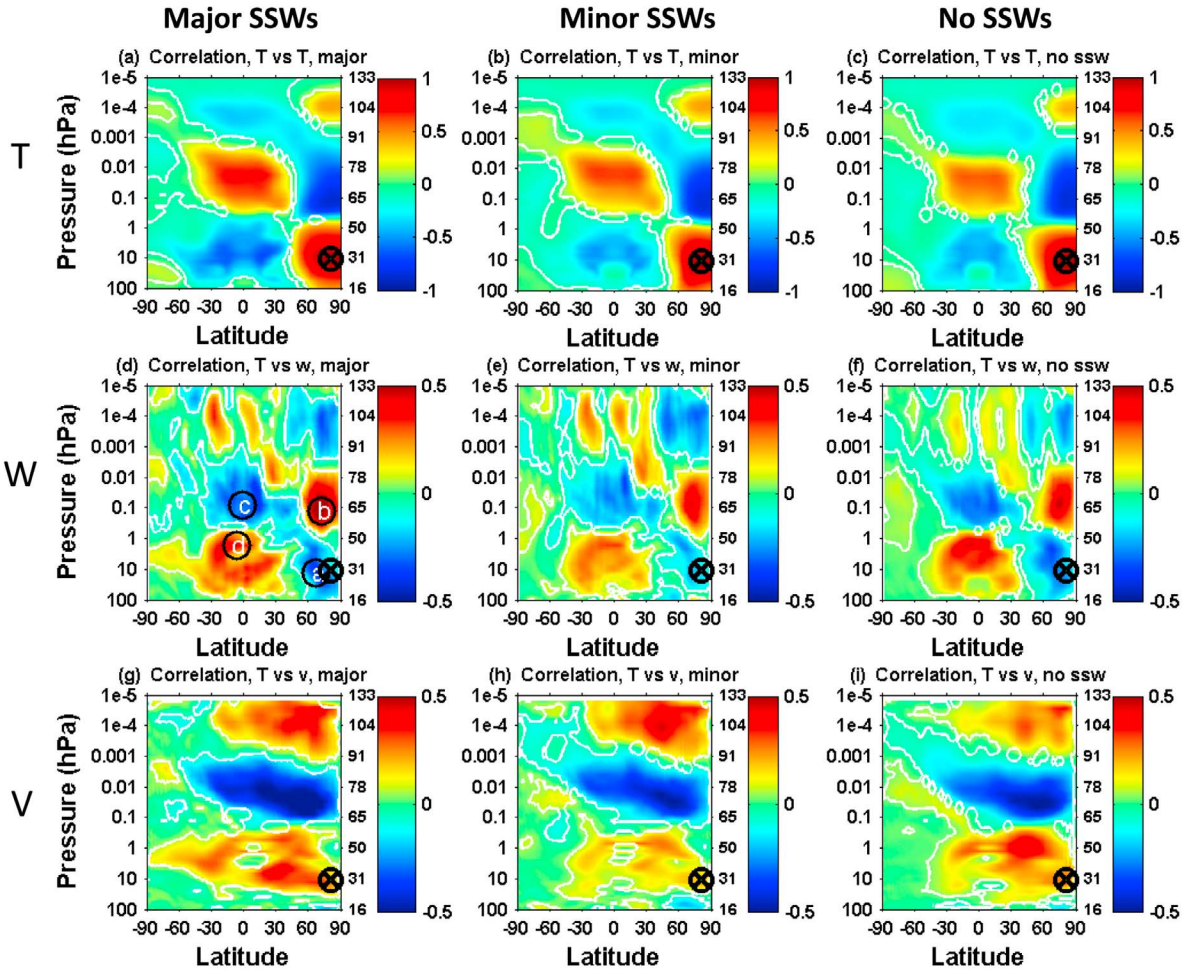

Figure 2. Correlation patterns between the WACCM (Oct 20–Mar 10) temperature anomalies at the reference point (10 hPa, 80°N) and anomalies of (top row) temperature T, (middle row) vertical wind W and (bottom row) meridional wind V associated with the residual circulations at all latitudes and altitudes for days with (left column) major SSWs, (middle column) minor SSWs and (right column) without SSWs. The correlation scale for T is −1 to 1 and the correlation scales for W and V are −0.5 to 0.5. The circle with a cross is the reference point used for the correlation calculations. White solid lines denote the 95% significance level.

anomalies are most significant during SSWs. Due to the 60-day yaw cycle of the TIMED spacecraft, SABER cannot cover the high latitudes in both hemispheres simultaneously, so no correlation is calculated poleward of 50°S in Figure 1.

[8] WACCM 3.5 simulation outputs during northern winter (from October 20 to March 10) are employed to reproduce the temperature correlation patterns and extend them to the global range from −90° to +90° in latitudes. The temperature anomalies of WACCM data from 1953 to 2006 are derived as the deviations from a long-term average for a given day at each latitude and altitude in a similar way as SABER, where the long-term average at that latitude and altitude is the mean over the 54 years of WACCM temperatures. The correlations of temperature anomalies are between a reference point at (10 hPa, 80°N) and all other latitudes and altitudes. The temperature correlation patterns for days with major SSWs, with minor SSWs and without SSWs are plotted in Figures 2a–2c. Here SSW events are identified using WACCM temperatures at the reference point. Temperature increases exceeding 25 K within three weeks are defined as SSWs, while the wind reversal at 10 hPa and 60°N is used to separate major and minor SSWs according to the World Meteorological Organization's definition.

[9] Comparing the temperature correlation results between WACCM and SABER, both show very similar patterns at high northern latitudes with positive correlation regions from 20 to 50 km, negative correlation regions from 55 to 90 km and positive correlation regions from 90 to 110 km. In the equatorial areas, both SABER and WACCM show a negative correlation region from 20 to 50 km and a positive correlation region from 50 to 90 km. Although this equatorial positive region in SABER has more structures than the result in WACCM, the correlations are significant as indicated by the 95% significant levels. A negative correlation region is also observed in the lower thermosphere from 90 to 110 km above the equator in WACCM, while in SABER this negative correlation is observed but the boundary of the region is not well defined. Such complicated correlation patterns of

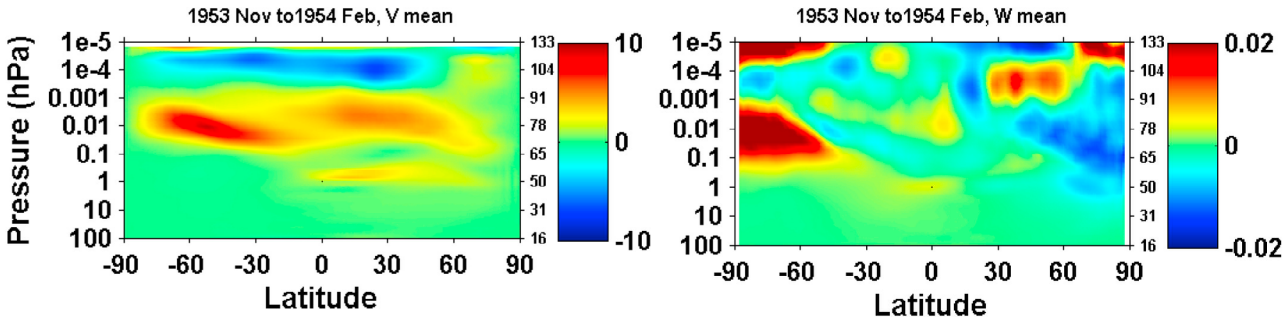

Figure 3. (left) Meridional wind V and (right) vertical wind W associated with the residual circulations computed from WACCM. The data were averaged from 1 Nov 1953 to 28 Feb 1954. The units for V and W are m/s. Northward and upward directions are defined as positive for V and W, respectively.

SABER from 70 to 110 km in the equatorial areas are likely due to the tidal aliasing effect as indicated by the alternated positive and negative correlations from 70 to 110 km. The observed temperature anomalies may contain components of tides and this may contaminate the correlation calculated. On the other hand, since the tides have been removed from the WACCM zonal means, the WACCM simulations give a very clear pattern of negative correlations in the lower thermosphere above the equatorial regions. As for the high northern latitudes, because the tidal amplitudes are generally smaller than in the equatorial regions, the aliasing effect is likely small enough so that SABER shows the clear positive correlation in the lower thermosphere from 90 to 110 km, which is very similar to the WACCM results. Overall the comparison demonstrates that WACCM resembles the SABER temperature correlation patterns quite well, confirming that WACCM resolves the underlying mechanisms of teleconnection.

[10] Besides the temperature correlations, the WACCM outputs are also used to derive the correlation patterns between the temperature anomalies at the reference point and the meridional (V) and vertical (W) components of the WACCM residual circulation anomalies (Figures 2d–2i). The circulation anomalies are derived in the same manner as the temperature anomalies. Here northward and upward directions are defined as positive for V and W, respectively. The correlation patterns of W in Figures 2d–2f correspond to the correlation patterns of temperature in Figures 2a–2c very well but with opposite signs and smaller magnitudes for the correlation coefficients. Note the change of the correlation scales in Figures 2d–2i. Such a correspondence is very clear for the three correlation regions at high northern latitudes and two regions in the equatorial stratosphere and mesosphere. The correlations of W versus T in the equatorial lower thermosphere exhibit more structures than those of T versus T, but in general have an opposite sign. Although the correlation magnitudes are small in the southern polar region, for the correlation regions with significance levels above 95%, the W versus T patterns still correspond with the T versus T patterns in opposite signs. To demonstrate the meanings of these correlations, we take the case of positive temperature anomaly as an example. When the temperature at the reference point increases, the positive (negative) temperature correlation represents the regions of heating (cooling). The corresponding negative (positive) correlation regions in the vertical wind patterns indicate the enhanced (reduced) downwelling or reduced (enhanced) upwelling. In the meantime, the positive (negative) correlations in the meridional wind patterns shown in Figures 2g–2i imply either the enhanced (reduced) northward wind or the reduced (enhanced) southward wind. The good correspondence between the W versus T patterns and the T versus T patterns confirms that adiabatic heating (cooling) controls the temperature anomalies.

3.2. Circulation Changes in the Stratosphere, Mesosphere and Lower Thermosphere

[11] The correlations of V versus T (Figures 2g–2i) exhibit three cell patterns from the stratosphere to the lower thermosphere. They reflect the changes of the residual circulations (Figure 3) that will be discussed in this section. The negative and positive correlation regions in the stratosphere as displayed in Figures 2a–2c are induced by the anomalies of the Brewer-Dobson circulation [*Körnich and Becker*, 2010]. The increase of planetary wave forcing in the northern stratosphere induces a stronger poleward Brewer-Dobson circulation [*Holton*, 1992; *Yulaeva et al.*, 1994], which is displayed as the positive response regions below 60 km in the correlation patterns of meridional wind in Figures 2g–2i. The stronger poleward circulation leads to an increase of downwelling (upwelling) in the northern polar (equatorial) stratosphere region, which is shown as negative (positive) correlations in Figures 2d–2f. Such increased downwelling (upwelling) results in enhanced adiabatic heating (cooling) in the polar (equatorial) stratosphere. The consequences are positive (negative) temperature correlations below 60 km in the corresponding regions as shown in Figures 2a–2c.

[12] Mesosphere correlation patterns in Figures 2a–2c are mainly induced by the anomalies of the summer-to-winter pole flow in the mesosphere. The increase of westward planetary-wave driving in the northern stratosphere decelerates the eastward wind in the winter stratosphere which in turn changes the filtering of gravity waves. Consequently, westward gravity wave forcing is reduced and thus the mesosphere summer-to-winter pole circulation is weakened [*Karlsson et al.*, 2009b; *Körnich and Becker*, 2010]. The decrease of this circulation is evident in the negative correlation of the meridional wind in Figures 2g–2i. The weakened circulation leads to weaker downwelling thus reduced adiabatic heating in the northern polar mesosphere, resulting

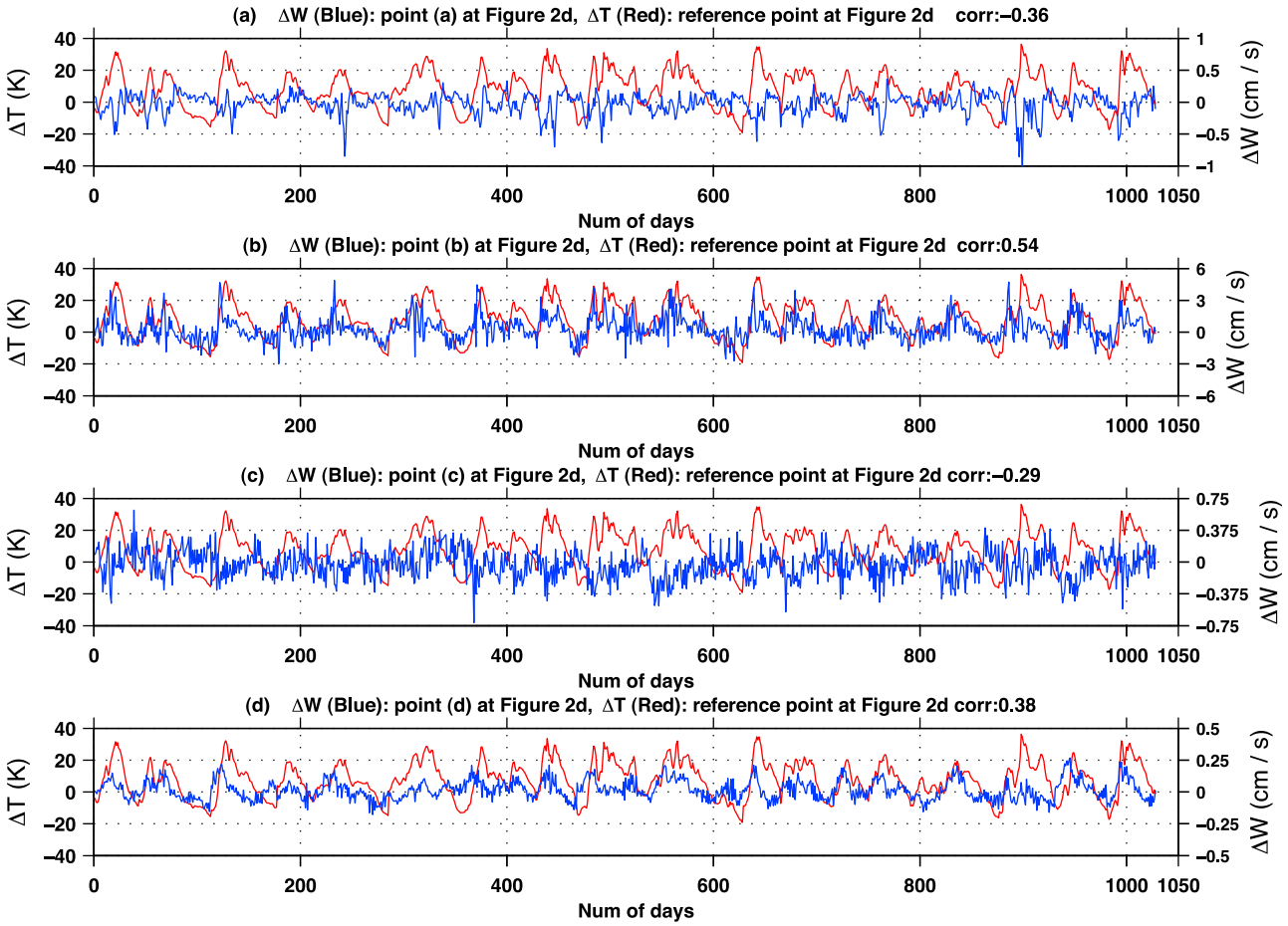

Figure 4. The time series of WACCM temperature anomalies (ΔT) (red solid line) at the reference point and the time series of WACCM vertical wind anomaly (ΔW) (blue solid lines) at four chosen points in Figure 2d. Figures 4a–4d correspond to the points a, b, c and d in Figure 2d, respectively.

in the negative temperature correlation from 55 to 90 km in Figures 2a–2c and positive vertical wind correlation in Figures 2d–2f in the same height range. In the equatorial mesosphere, the increasing temperature corresponds to the enhanced adiabatic heating or reduced adiabatic cooling associated with the negative anomalies of vertical wind according to Figures 2d–2f. Vertical wind anomalies in the equatorial mesosphere are manifested either as an increase of downwelling or a decrease of upwelling, but whether or not these anomalies of downwelling or upwelling are caused by the meridional mesospheric circulation anomalies deserves further study in the future. Figures 2g–2i show that the negative correlation regions of the meridional circulation in the mesosphere extend from the northern polar region to ~50°S, suggesting that the mesosphere response to the winter stratosphere anomalies is a global effect. That is, the winter stratosphere anomalies are able to cross the equator and affect the mesosphere at southern midlatitudes through the circulation, for which the underlying mechanisms need future investigations.

[13] According to the residual circulation calculated from WACCM (Figure 3), there is a winter-to-summer circulation in the lower thermosphere (above 95 km). As illustrated in Figures 2d–2i, the change of this winter-to-summer circulation in the lower thermosphere responds to the temperature anomalies in the northern stratosphere and produces the equatorial negative temperature correlation and the positive temperature correlation in the northern polar regions from 90 km to 120 km in Figures 2a–2c. Likely associated with the weakening of the summer-to-winter circulation in the mesosphere, this winter-to-summer circulation in the lower thermosphere also weakens and leads to temperature anomalies in the corresponding regions through adiabatic heating/cooling.

[14] The results presented here show that the modeled temperature anomalies in the winter polar stratosphere are correlated with temperature and circulation anomalies at all latitudes between 15 and 110 km. Although the correlation coefficients at the high southern latitudes are small in Figure 2, the majority of them are statistically significant as indicated by the significance levels being above 95%. The small magnitudes of the southern correlation coefficients are most likely due to the inter- and intra-annual variations of the correlation patterns, as will be discussed in Section 3.3. Figures 2g–2i show that all the circulations are affected by the anomalies in the winter polar stratosphere: the Brewer-Dobson circulation in the stratosphere, the summer-to-winter circulation in the mesosphere and the winter-to-summer circulation in the lower thermosphere. Changes in the circulations are responsible for the correlation patterns in the

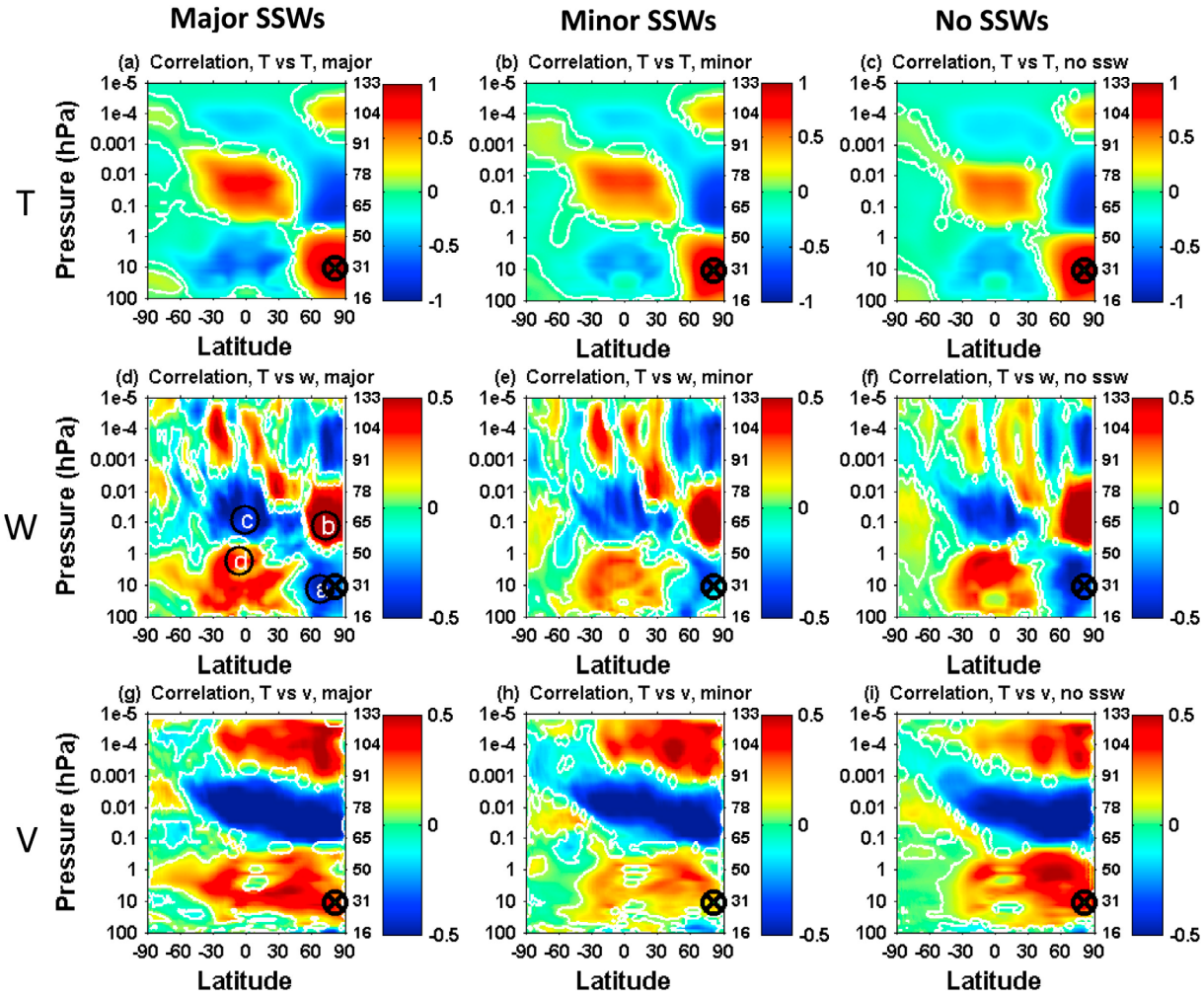

Figure 5. Similar to Figure 2, but the correlation patterns are calculated using the vertical wind and meridional wind smoothed over 10 days.

corresponding regions. Therefore, the temperature correlation patterns can be used as a proxy to identify the range and boundary of the circulations.

[15] To directly examine the correlations between the residual circulation and temperature, we compare in Figure 4 the vertical wind time series taken at 4 different locations (a, b, c and d in Figure 2d) with the temperature time series at the reference point. The time series are formed by splicing together segments of temperature and wind every winter during the period of SSW, which is the same method used in forming time series in the calculation of Figure 2. The positive or negative correlations between the anomalies of the two quantities are convincing, and all four correlations have the significance levels above 99%. The correlations become even more evident when the wind data are smoothed over 10-days for every year before spliced together so short-period fluctuations (periods of several days) are removed. The correlation coefficients are recalculated using the smoothed winds and the results are displayed in Figure 5. After the smoothing, the correlation patterns are nearly identical to the unsmoothed patterns shown in Figure 2 but with larger magnitudes of correlation coefficients in most regions. These tests confirm the existence of the correlations between temperature and vertical wind derived above. Figure 5 further suggests that the correlations exist in the multiday periods more strongly than in the day-to-day variations.

3.3. Teleconnection Patterns Versus SSW, Inter-annual and Intra-annual Variability

[16] According to Figure 2, the correlation patterns from WACCM for the days with major SSWs, with minor SSWs and without SSWs are nearly identical. In Figure 1, the correlations from SABER for days with and without SSWs also have similar patterns. These results provide evidence that temperature anomalies during the periods of major SSWs, minor SSWs and no SSWs are all induced by anomalies of the planetary-wave driven branch of the residual circulation in the winter stratosphere. The differences among these three cases are in the amplitudes and signs of planetary wave anomalies and temperature perturbations. Strong positive perturbations show up as SSWs, while other perturbations are not considered as SSW. Our results are in agreement with a finding in CMAM by *Karlsson et al.* [2009a] that either sign of the vertical component of the Eliassen-Palm flux in the winter stratosphere leads to the similar inter-hemispheric coupling patterns.

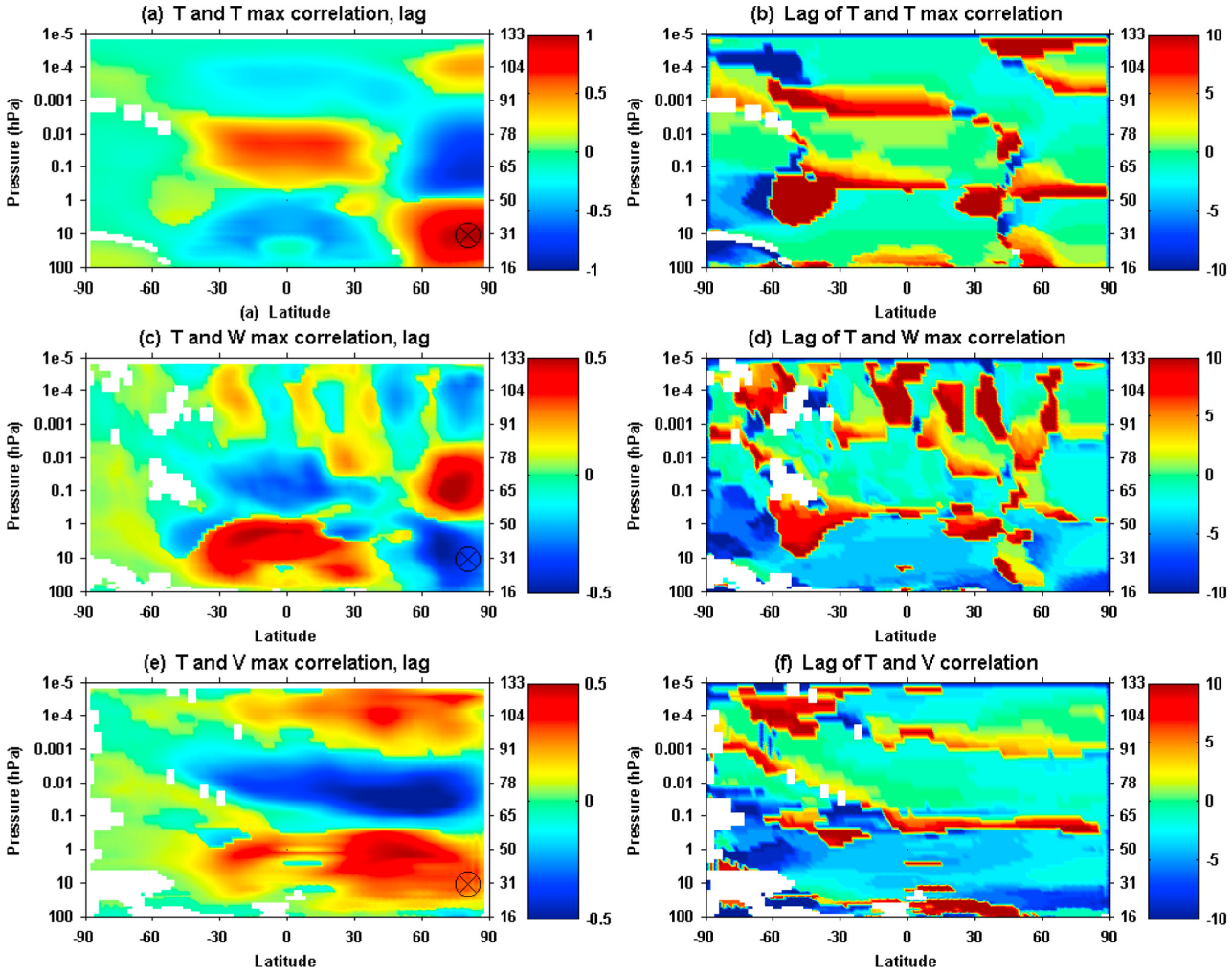

Figure 6. The maximum correlation coefficients for (a) temperature (T), (c) vertical wind (W) and (e) meridional wind (V) obtained within the time lags of −10 to +10 days. (b, d, and f) The time lags corresponding to the maximum correlation coefficients. The insignificant points have been removed from all plots and appear as white spots or areas.

[17] We notice in Figure 2 that the correlation magnitudes in the SH poleward of 60°S are relatively small when compared to the previous studies by, e.g., *Karlsson et al.* [2009a] and *Xu et al.* [2009]. Several factors may have contributed to the weak correlations in the southern polar region in the current study, including the time lag, the different reference point used in the current study, the intra-annual and inter-annual variations of correlation regions. We examine these factors one by one in the following.

[18] In previous studies, *Becker and Fritts* [2006] suggested a time lag of ∼1 month for the SH mesosphere temperature anomaly to respond to the NH planetary wave anomaly. *Karlsson et al.* [2009a] showed in the CMAM that the response time of the SH temperature to the NH planetary wave was 15–20 days while the temperature-to-temperature response time between two hemispheres was instantaneous. Using the MLS data, *Xu et al.* [2009] showed a temperature-to-temperature response time ranging from 1 to 7 days at different correlation regions. To study the effects of time lag on the derived correlation patterns in Figure 2, we calculate the correlation coefficients for the time lags ranging from −10 days to +10 days relative to the temperatures at the reference point. The results are displayed in Figure 6. It is worth to point out that the time series used in Figure 6 are formed by simply joining 54 years of winter temperature or wind data together without separating them into different periods of major, minor and no SSWs. Figures 6a, 6c and 6e illustrate the maximum correlations obtained within the lags of −10 to +10 days, while the associated time lags for achieving the maximum correlations are plotted in Figures 6b, 6d and 6f. The maximum correlation patterns of T versus T in Figure 6a are nearly identical to the patterns of Figures 2a–2c with zero lags. They all show strong correlations in the NH and equatorial regions but weak correlations in the SH poleward of 60°S. As a result, we conclude that the time lag is not the cause of the weak correlations in the southern polar region plotted in Figure 2. Furthermore, the time lags shown in Figure 6b for the regions with relatively large positive or negative correlations are close to zero, indicating that the temperature-to-temperature responses are instantaneous

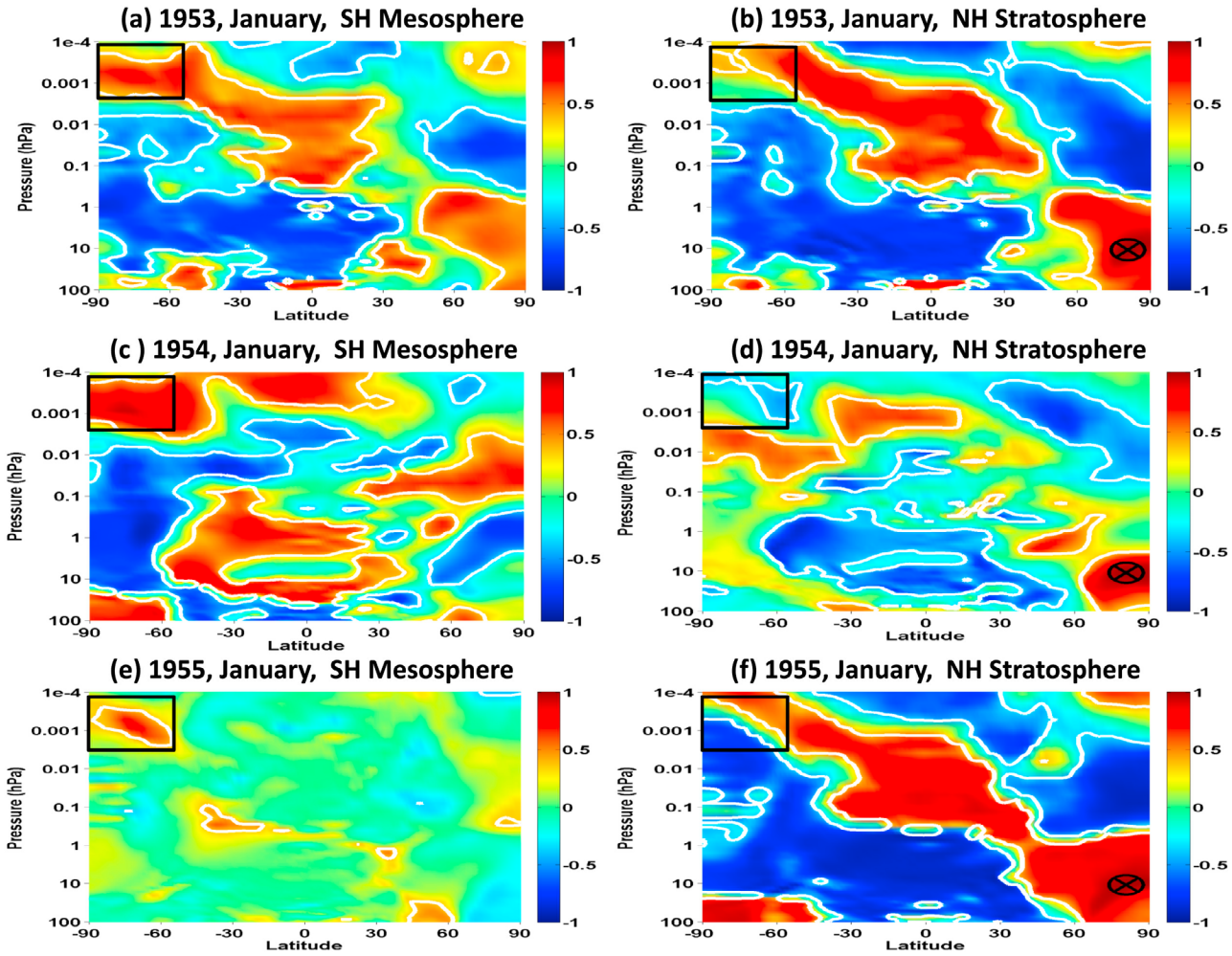

Figure 7. Correlation patterns of WACCM temperatures for January 1953, 1954 and 1955. (a, c, and e) The reference points are located in the southern mesosphere (averaged from 50°S to 90°S and from 0.00012 to 0.004 hPa), similar to the reference point used in Figure 1a of *Karlsson et al.* [2009a]. (b, d, and f) The reference points are located in the northern stratosphere, marked as circles with crosses. White solid lines denote the 95% significance level.

north of 60°S. Some large lag values show up in Figure 6b for the regions with small correlation magnitudes. Such lags should be discarded in the analysis because the correlations are fluctuated around 0, resulting in meaningless lags. The maximum correlation patterns of T versus W in Figure 6c and of T versus V in Figure 6e are similar to the corresponding correlation patterns with zero lags in Figures 2d–2f and Figures 2g–2i, respectively. Again, the time lags have very little effects on the correlation patterns. Interestingly, the time lags from 100 hPa to 0.001 hPa in the equatorial and northern hemisphere regions in Figures 6d and 6f are negative in general, indicating that the W and V wind anomalies lead the temperature anomaly at the reference point by 2 to 10 days. This time lag of 2–10 days is smaller than the lag of temperature response to the planetary wave anomaly (15 days to 1 month) but larger than the lag of temperature response to temperature anomaly (instantaneous–7days) in the northern stratosphere. Such a result is anticipated because the planetary wave anomaly occurs first and induces the residual circulation anomaly. The residual circulation anomaly in turn leads to the temperature anomaly that occurs last in the sequence.

[19] The reference point chosen in the northern stratosphere to calculate the correlations in the current study is different than the southern mesosphere reference used in previous studies. To investigate whether the reference point plays a role in the correlation magnitudes, we calculate the correlation patterns for January of 1953–1955 using both reference points in Figure 7. On the left, Figures 7a, 7c and 7e employ a reference point in the southern mesosphere (averaged from 50°S to 90°S and from 1.2×10^{-4} hPa to 4×10^{-3} hPa), similar to that used in Figure 1a of *Karlsson et al.* [2009a]. The area used to calculate the reference point is marked as a black rectangle in each plot. On the right, Figures 7b, 7d and 7f use the same reference point in the northern stratosphere as Figure 2. Figures 7a and 7b show very similar correlation patterns; however, Figures 7c and 7d exhibit the opposite correlations in general. Comparing Figure 7e with Figure 7f, while Figure 7f using the NH stratosphere reference point gives clear correlation pattern

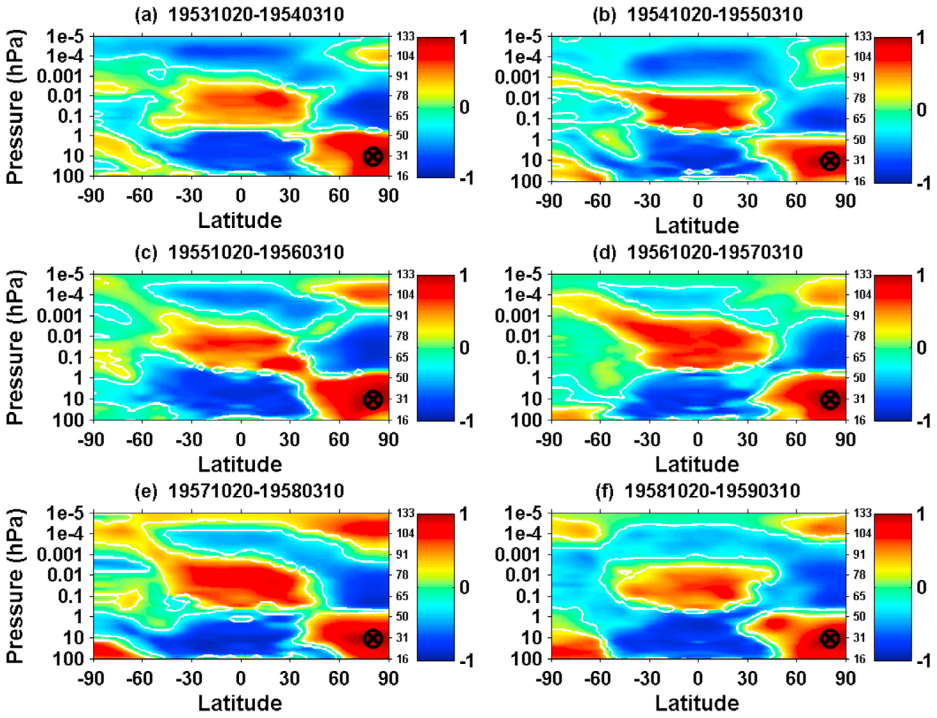

Figure 8. Correlation patterns between the WACCM temperature anomalies at the reference point (10 hPa, 80°N) and at all latitudes and altitudes for the winters from 1953 to 1958. The title of each subplot gives the dates of data period in the format of "yyyymmdd–yyyymmdd." The circle with a cross is the reference point used for the correlations. White solid lines denote the 95% significance level.

with large correlation magnitudes, Figure 7e using the SH mesosphere reference point gives very small correlations globally. The puzzling results above can be explained by the height variations of the correlation regions in the southern polar region. In Figure 7b, the reference point in the NH stratosphere and the reference point area in the SH mesosphere (inside the black rectangle) are positively correlated, leading to the similar correlation patterns of Figures 7a and 7b. According to Figure 7d, the temperature anomalies at two reference points are anti-correlated; therefore, Figures 7c and 7d have opposite signs of correlation patterns. In Figure 7f, half of the reference point area in the SH mesosphere is positively correlated with the reference point in the NH stratosphere while the other half is anti-correlated. Consequently, Figure 7e does not show clear correlation patterns when the reference point rectangle in the SH mesosphere is used. Regarding the high southern latitudes, Figures 7b and 7f show that the large correlations (nearly 1) are achieved in the SH poleward of 60°S using the single year and single month data with the reference point in the NH stratosphere. This means that the reference point chosen in this study is not the cause of small correlation coefficients in the southern polar region. Furthermore, the results shown in Figure 7 indicate the advantages of choosing a reference point in the NH stratosphere. That is, despite some changes in the SH polar region in Figure 7d, the patterns in the equatorial and NH regions are stable and consistent in Figures 7b, 7d and 7f. Such advantages can be seen even more clearly in the inter-annual and intra-annual variations of correlation regions to be discussed below.

[20] To study the inter-annual variations of teleconnection, the temperature correlation patterns are calculated from WACCM for individual years from 1953 to 2006. Regions with significant positive and negative correlations exist poleward of 60°S each year, but the altitudes of these regions vary from year to year through all 54 years. Figure 8 illustrates the yearly correlation patterns from 1953 to 1958 as examples. For the winters of 1953–1954 and 1954–1955, a positive correlation region with a significance level above 95% occurred poleward of 60°S in the altitude range of 80–90 km. However, it moved to 90–100 km in the winter of 1956–1957. For the winters of 1957–1958 and 1958–1959, the positive correlation region was located even above 100 km. Similarly, the negative and positive correlation regions below 80 km exhibit inter-annual altitude variations at the latitudes poleward of 60°S. Indeed, the inter-annual variations have shown up in Figure 7 where using the January data and a reference point in the NH stratosphere, the correlation regions in the southern polar region have different altitudes every year, further confirming the existence of inter-annual variations. Therefore, when averaged over multiple years, the correlations in the SH poleward of 60°S are largely canceled out due to the inter-annual variations. A direct consequence is the correlations calculated in the current study being small in the SH poleward of 60°S as shown in Figure 2. In contrast, the positive and negative correlation regions in the equatorial and NH regions are quite consistent over the years, leading to the clear patterns after multiple-year averaging. These facts also demonstrate the advantage of stable patterns around the equator and in the NH when a

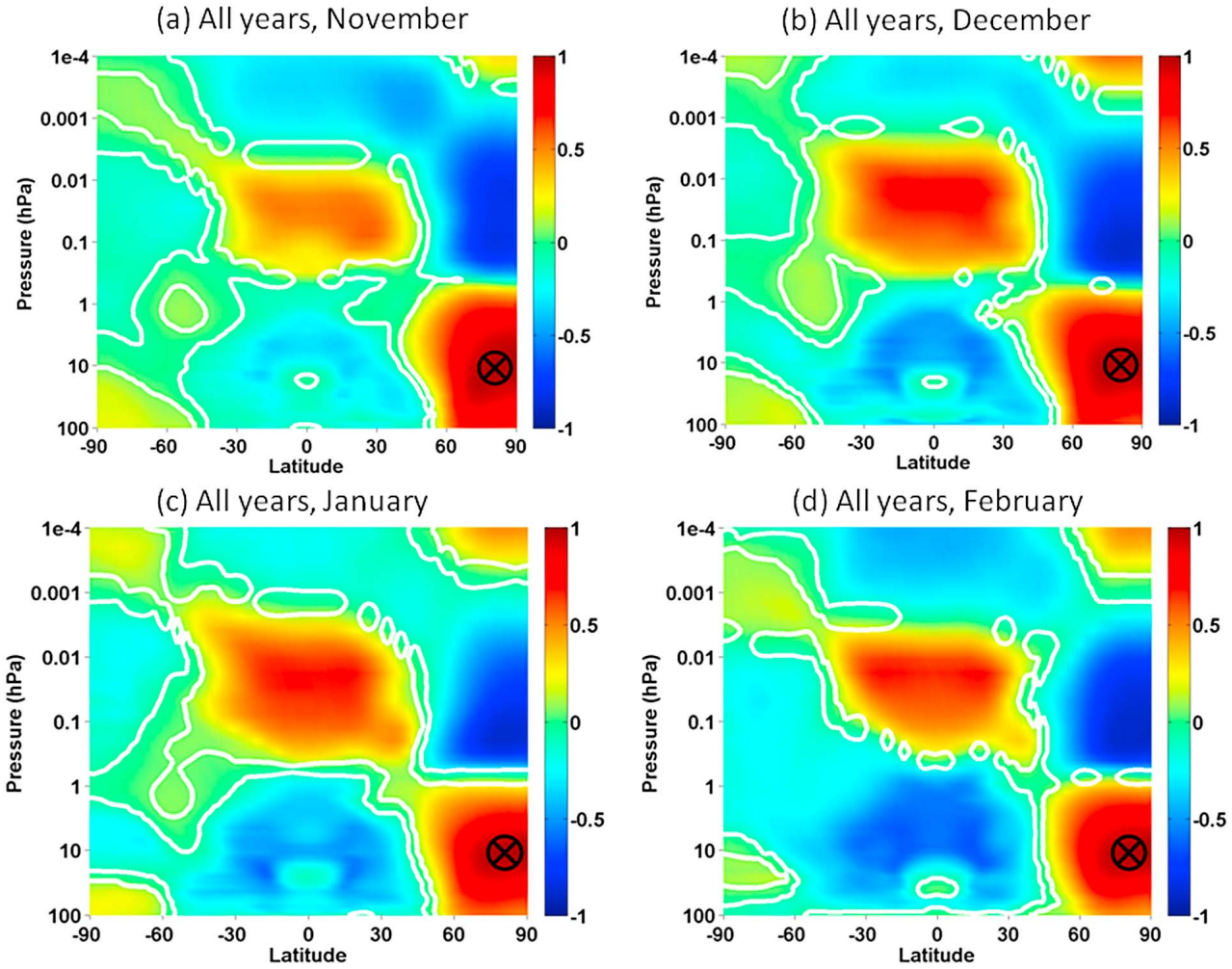

Figure 9. Correlation patterns between the WACCM temperature anomalies at the reference point (10 hPa, 80°N) and temperature anomalies at all latitudes and altitudes for (a) November, (b) December, (c) January and (d) February. The circle with a cross is the reference point used for the correlation calculations. White solid lines denote the 95% significance level.

reference point in the NH stratosphere is chosen in the correlation studies.

[21] In addition to the inter-annual variability, the results in Figures 7 and 8 also indicate the intra-annual variations. The correlation patterns for January 1955 (Figure 7f) show strong correlations at the high southern latitudes; however, the correlation patterns for the entire winter from 20 October 1954 to 10 March 1955 (Figure 8) give much weaker correlations at the same latitudes. This difference can be easily explained by the altitude variations from November through February, as the correlations are largely smoothed out when 4 winter months are combined together. To further investigate the intra-annual variations, the monthly correlation patterns are calculated using all 54 years of WACCM data and the results are displayed in Figure 9. The time series used in Figure 9 are formed via splicing together the 54 years of temperature data in each of the months (November through February). The intra-annual altitude variations of the correlation regions are obvious at the high southern latitudes. Three correlation regions with the significance levels above 95% (i.e., the positive correlation from $\sim 1 \times 10^{-3}$ to 1×10^{-4} hPa, the negative correlation from $\sim$10 to 0.001 hPa, and the positive correlation from about 100 to 10 hPa) in the SH poleward of 60°S all have altitudes varying from one month to another. The intra-annual variations of correlation pattern altitudes cause the correlations at the high southern latitudes to be smoothed out when the correlations are calculated for all the winter months. Therefore, the intra-annual variations likely contribute to the weak correlations in the southern polar region shown in Figures 2 and 5. Note that the correlation patterns in the equatorial and NH regions are located at the same altitudes from the stratosphere to the lower thermosphere for all winter months, suggesting the advantage of choosing a reference point in the northern polar stratosphere.

[22] In summary, the time lag is not the reason of weak correlations at the high southern latitudes. The reference point in the northern stratosphere has the advantage to show stable teleconnection patterns in the equatorial and NH regions, but it is not the cause of weak correlations in the southern polar region. The inter-annual and intra-annual altitude variations of the correlation regions are most likely responsible for the weak correlations at the high southern

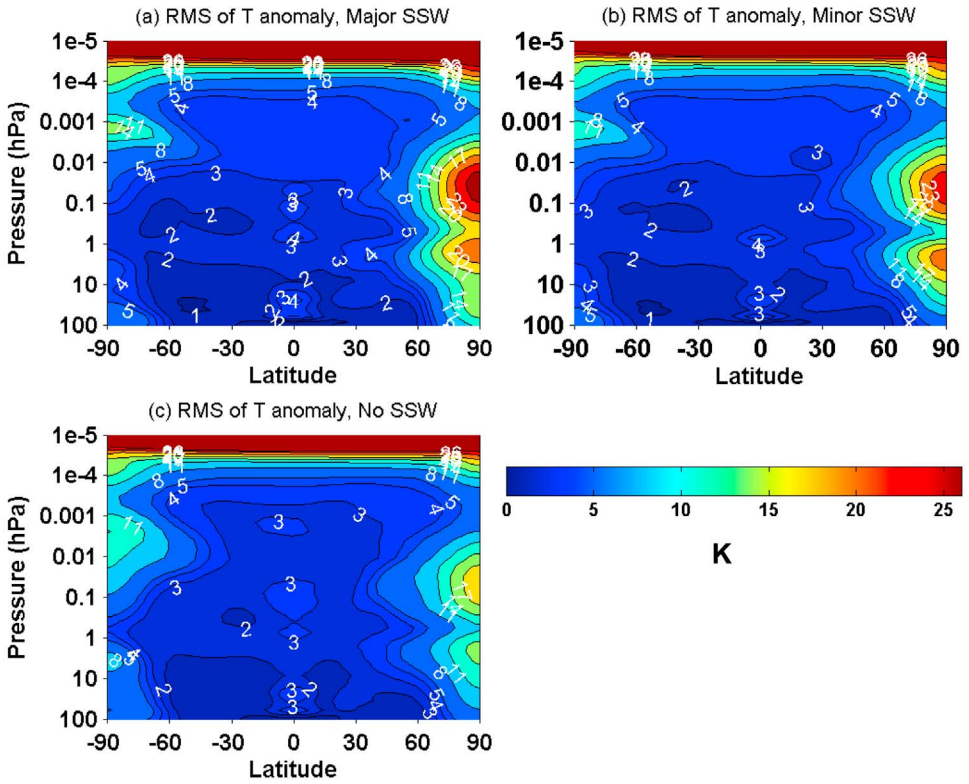

Figure 10. RMS magnitudes of temperature anomalies (unit: K) during (a) major, (b) minor and (c) no SSWs.

latitudes. It is worth to point out that time series of daily and zonally averaged data from WACCM are used to calculate the correlation patterns in this study, while *Karlsson et al.* [2009a] used monthly and zonally averaged data from CMAM. The WACCM results do not necessarily represent a difference to the teleconnection in the CMAM.

3.4. Magnitudes of Temperature Anomalies

[23] It is of interest to quantify the magnitudes of temperature anomalies under different SSW conditions. We take the time series of WACCM temperature anomalies (like the example shown as the red lines in Figure 4) for each location and compute its root-mean square (RMS) value. The result represents the RMS magnitude of temperature anomalies at that location. Such computation is repeated for major, minor and no SSWs, respectively. The resulted global maps of RMS magnitude versus latitude and altitude are displayed in Figure 10. The RMS magnitudes at the northern polar region reach local maxima around 0.1 hPa and 5 hPa. At the southern polar MLT region, the RMS magnitudes reach a local maximum around 0.001 hPa with values of 14, 11 and 11 K for major, minor and no SSWs, respectively. Around equatorial regions, the RMS magnitudes of temperature anomalies are less than 5 K below the thermosphere. In general, the magnitudes of temperature anomalies during major SSWs are larger than those during minor and no SSWs. To some extent, these RMS magnitudes of temperature anomalies indicate the temperature responses to different SSW conditions. But cautions must be taken when interpreting the results, because altitude variations and annual variations may obscure the temperature anomalies to reveal the real temperature responses.

4. Conclusions and Discussion

[24] We have established the teleconnection patterns of temperature anomalies in the northern polar stratosphere with temperature or wind anomalies at global latitudes and altitudes from 15 to 110 km using SABER temperature data and WACCM simulations of zonally and daily averaged temperatures and winds. The correlation patterns show that teleconnection exists globally over the entire equatorial, mid- and high-latitudes and from the stratosphere to the lower thermosphere. Along with previous studies, these two new data sets further demonstrate the robustness of the teleconnection pattern and its role as an important atmospheric coupling mechanism. The correlation patterns between the temperature anomalies and residual circulation anomalies are established using the WACCM simulations. The WACCM correlation patterns reveal that temperature anomalies from the stratosphere to the thermosphere correspond well to the corresponding anomalies of residual circulations through adiabatic heating and cooling. These circulation anomalies are induced by planetary wave anomalies in the northern polar stratosphere. Since the residual circulations have clear responses to the anomalies and form different correlation regions, the correlation patterns may be used as a proxy to identify the boundaries of the circulations.

[25] A main new finding of this study is that the teleconnection extends well into the lower thermosphere and the thermospheric anomalies are consistent with the corresponding

changes of the winter-to-summer lower-thermospheric branch of the residual circulation. Although this is the first report in which the teleconnection between the stratosphere and the thermosphere is clearly identified, we notice that Figures 4b and 4d in *Karlsson et al.* [2009b] derived from MLS temperature data hint some coupling between the thermosphere and the stratosphere, thus another data set supporting our finding. Our results demonstrate that the stratosphere perturbations can have strong influences on the thermosphere via teleconnection, which may have important implications to the thermosphere research. For example, the temperature perturbations will lead to the changes in the thermosphere density, affecting space weather, especially the satellite drag. The changes in the thermospheric residual circulation will influence the constituent transport, e.g., affecting the $[O]/[N_2]$ ratio that can impact the ionosphere via various processes.

[26] We have examined the teleconnection for time periods with and without SSWs using a reference point chosen in the northern winter stratosphere in order to be consistent with the definition of a SSW. It is found that the teleconnection patterns do not depend on the presence of SSWs. That is, the teleconnection structures for time periods with and without SSWs display similar patterns in SABER, and teleconnection patterns in WACCM are nearly identical for days with major SSWs, minor SSWs and without SSWs. Such similarities occur in the correlation patterns of temperature versus temperature and also of temperature versus residual circulation. These results indicate that major SSWs, minor SSWs and small temperature anomalies are likely caused by similar mechanisms but with different magnitudes; that is, anomalies of circulations driven by planetary waves in the winter stratosphere.

[27] The current study using WACCM simulations discovers strong inter-annual and intra-annual altitude variations of the teleconnection patterns in the southern polar region but stable altitudes of correlation regions in the equatorial and northern latitudes. The correlation magnitudes in the SH poleward of 60°S are relatively small in the current study when compared to the previous studies by, e.g., *Karlsson et al.* [2009a] and *Xu et al.* [2009]. Our investigations of the weak correlations conclude the following. The time lag is not the reason of weak correlations at the high southern latitudes. The reference point in the northern stratosphere has the advantage to show clear and stable teleconnection patterns in the equatorial and NH regions when 54 years of data are combined together to calculate the correlation patterns, and it is not the cause of weak correlations in the southern polar region. The inter-annual and intra-annual altitude variations of the correlation regions are most likely responsible for the weak correlations at the high southern latitudes. This is because the positive and negative correlations are largely canceled out when the correlation patterns are averaged over 54 years or over 4 winter months, although single year and single month data yield large correlations in the southern polar region.

[28] The time lag has very little effects on the teleconnection patterns as shown by the current study; however, our time lag analysis indicates that from 100 to 0.001 hPa in the equatorial and northern hemisphere regions, the vertical and meridional wind anomalies lead the temperature anomaly at the reference point by 2 to 10 days. This time lag is smaller than the lag of temperature response to the planetary wave anomaly (15 days to 1 month) but larger than the lag of temperature response to temperature anomaly (instantaneous–7 days) in the northern stratosphere. Such a result suggests that the planetary wave anomaly occurs first and induces the residual circulation anomaly. The residual circulation anomaly in turn leads to the temperature anomaly that occurs last in the sequence.

[29] We believe that the current study with SABER and WACCM has effectively broadened and furthered our understanding of the global teleconnection phenomena and possible underlying mechanisms. The correlation patterns in the region from 50°S to the North Pole are stable from year to year, within a year and with various SSW intensities in WACCM. It implies that the first two stages of the inter-hemispheric coupling mechanism as outlined in *Körnich and Becker* [2010], which are responsible for the correlation patterns northward of 50°S, are generally stable. On the other hand, the third stage of the coupling, where the perturbation propagates through the mesosphere and lower thermosphere from the equator to the summer pole, is much more variable, particularly poleward of 60°S, and this leads to the strong inter- and intra-annual altitude variations in the southern polar region as found by the current study. Nevertheless, there are still considerable issues to be addressed in the future studies and we have identified several in Section 3. Furthermore, the origin of the inter-annual and intra-annual variations of the correlation patterns in the southern polar region deserves good attentions. One possible mechanism is the intrahemispheric coupling proposed by *Karlsson et al.* [2011]. Variations in the timing of the late-spring breakdown of the stratospheric polar vortex in the SH [*Langematz and Kunze*, 2008] may influence the propagation of gravity waves up to the mesosphere, thus adding an intrahemispheric control from the stratosphere to the MLT temperature. This is additional to the inter-hemispheric coupling discussed above. When a reference point is chosen in the northern polar winter stratosphere as we did in the current study, only if the anomalies in the southern MLT region is mainly controlled by the anomalies of the planetary-wave driven branch of the residual circulation (that is, the inter-hemispheric coupling), will the correlation regions occur with stable altitudes in the southern MLT. It is possible that the intrahemispheric waves within the southern polar region strongly influence the southern MLT region, leading to the large altitude variations of the correlation regions in different months or years. Using a reference point in the northern winter stratosphere may help the studies of intrahemispheric coupling by revealing the variations of correlation regions under different dynamic conditions.

[30] **Acknowledgments.** We sincerely acknowledge the valuable comments by Anne K. Smith, Erich Becker, two anonymous reviewers and Jonathan S. Friedman. B.T. was supported and X.C. and C.Y. were partially supported by NSF grant ATM-0645584. H.L.L.'s research is partially supported by NASA LWS Strategic Capability grant NNX09AJ83G and NSF CEDAR grant ATM-0836386. C.Y. acknowledges the support of NCAR Newkirk Graduate Fellowship. J.R. was supported by NASA's small Explorers Program under contract NAS5–03132. The National Center for Atmospheric Research is sponsored by the National Science Foundation.

References

Andrews, D. G., J. R. Holton, and C. B. Leovy (1987), *Middle Atmosphere Dynamics*, Academic, San Diego, Calif.

Balachandran, N., and D. Rind (1995), Modeling the effects of UV variability and the QBO on the troposphere-stratosphere system. Part I. The middle atmosphere, *J. Clim.*, *8*, 2058–2079, doi:10.1175/1520-0442(1995)008<2058:MTEOUV>2.0.CO;2.

Becker, E., and D. C. Fritts (2006), Enhanced gravity-wave activity and interhemispheric coupling during the MaCWAVE/MIDAS northern summer program 2002, *Ann. Geophys.*, *24*(4), 1175–1188, doi:10.5194/angeo-24-1175-2006.

Becker, E., and G. Schmitz (2003), Climatological effects of orography and land-sea heating contrasts on the gravity wave-driven circulation of the mesosphere, *J. Atmos. Sci.*, *60*(1), 103–118, doi:10.1175/1520-0469(2003)060<0103:CEOOAL>2.0.CO;2.

Becker, E., A. Müllemann, F.-J. Lübken, H. Körnich, P. Hoffmann, and M. Rapp (2004), High Rossby-wave activity in austral winter 2002: Modulation of the general circulation of the MLT during the MaCWAVE/MIDAS northern summer program, *Geophys. Res. Lett.*, *31*, L24S03, doi:10.1029/2004GL019615.

Espy, P. J., S. Ochoa Fernández, P. Forkman, D. Murtagh, and J. Stegman (2011), The role of the QBO in the inter-hemispheric coupling of summer mesospheric temperatures, *Atmos. Chem. Phys.*, *11*(2), 495–502, doi:10.5194/acp-11-495-2011.

Garcia, R. R., D. R. Marsh, D. E. Kinnison, B. A. Boville, and F. Sassi (2007), Simulation of secular trends in the middle atmosphere, 1950–2003, *J. Geophys. Res.*, *112*, D09301, doi:10.1029/2006JD007485.

Gumbel, J., and B. Karlsson (2011), Intra- and inter-hemispheric coupling effects on the polar summer mesosphere, *Geophys. Res. Lett.*, *38*, L14804, doi:10.1029/2011GL047968.

Holton, J. R. (1992), *An Introduction to Dynamic Meteorology*, Academic, San Diego, Calif.

Karlsson, B., H. Körnich, and J. Gumbel (2007), Evidence for interhemispheric stratosphere-mesosphere coupling derived from noctilucent cloud properties, *Geophys. Res. Lett.*, *34*, L16806, doi:10.1029/2007GL030282.

Karlsson, B., C. McLandress, and T. G. Shepherd (2009a), Inter-hemispheric mesospheric coupling in a comprehensive middle atmosphere model, *J. Atmos. Sol. Terr. Phys.*, *71*, 518–530, doi:10.1016/j.jastp.2008.08.006.

Karlsson, B., C. E. Randall, S. Benze, M. Mills, V. L. Harvey, S. M. Bailey, and J. M. Russell (2009b), Intra-seasonal variability of polar mesospheric clouds due to inter-hemispheric coupling, *Geophys. Res. Lett.*, *36*, L20802, doi:10.1029/2009GL040348.

Karlsson, B., C. E. Randall, T. G. Shepherd, V. L. Harvey, J. Lumpe, K. Nielsen, S. M. Bailey, M. Hervig, and J. M. Russell III (2011), On the seasonal onset of polar mesospheric clouds and the breakdown of the stratospheric polar vortex in the Southern Hemisphere, *J. Geophys. Res.*, *116*, D18107, doi:10.1029/2011JD015989.

Körnich, H., and E. Becker (2010), A simple model for the interhemispheric coupling of the middle atmosphere circulation, *Adv. Space Res.*, *45*(5), 661–668, doi:10.1016/j.asr.2009.11.001.

Langematz, U., and M. Kunze (2008), Dynamical changes in the Arctic and Antarctic stratosphere during spring, in *Climate Variability and Extremes During the Past 100 Years*, edited by S. Brönnimann et al., pp. 293–301, Springer, Dordrecht, Netherlands, doi:10.1007/978-1-4020-6766-2_20.

Remsberg, E. E., L. L. Gordley, B. T. Marshall, R. E. Thompson, J. Burton, P. Bhatt, V. L. Harvey, G. Lingenfelser, and M. Natarajan (2004), The Nimbus 7 LIMS version 6 radiance conditioning and temperature retrieval methods and results, *J. Quant. Spectrosc. Radiat. Transfer*, *86*(4), 395–424, doi:10.1016/j.jqsrt.2003.12.007.

Richter, J. H., F. Sassi, R. R. Garcia, K. Matthes, and C. A. Fischer (2008), Dynamics of the middle atmosphere as simulated by the Whole Atmosphere Community Climate Model, version 3(WACCM3), *J. Geophys. Res.*, *113*, D08101, doi:10.1029/2007JD009269.

Richter, J. H., F. Sassi, and R. R. Garcia (2010), Towards a physically based gravity wave source parameterization in a general circulation model, *J. Atmos. Sci.*, *67*, 136–156, doi:10.1175/2009JAS3112.1.

Russell, J. M., III, M. G. Mlynczak, L. L. Gordley, J. J. Tansock Jr., and R. W. Esplin (1999), Overview of the SABER experiment and preliminary calibration results, *Proc. SPIE Int. Soc. Opt. Eng.*, *3756*, 277, doi:10.1117/12.366382.

Xu, X., A. H. Manson, C. E. Meek, T. Chshyolkova, J. R. Drummond, C. M. Hall, D. M. Riggin, and R. E. Hibbins (2009), Vertical and inter-hemispheric links in the stratosphere-mesosphere as revealed by the day-to-day variability of Aura-MLS temperature data, *Ann. Geophys.*, *27*(9), 3387–3409, doi:10.5194/angeo-27-3387-2009.

Yulaeva, E., J. R. Holton, and J. M. Wallace (1994), On the cause of the annual cycle in tropical lower-stratospheric temperatures, *J. Atmos. Sci.*, *51*(2), 169–174, doi:10.1175/1520-0469(1994)051<0169:OTCOTA>2.0.CO;2.